Journal of Zhejiang University-SCIENCE A (Applied Physics & Engineering) 2022 23(1):27-39
www.jzus.zju.edu.cn; www.springer.com/journal/11582
E-mail: jzus_a@zju.edu.cn

Research Article

https://doi.org/10.1631/jzus.A2100192

Aerodynamic performance of distributed electric propulsion with wing interaction

Yao LEI[1,2]✉, Wen-jie YANG[1], Yi-yong HUANG[1]

[1]*School of Mechanical Engineering and Automation, Fuzhou University, Fuzhou 350116, China*
[2]*Key Laboratory of Fluid Power and Intelligent Electro-Hydraulic Control (Fuzhou University), Fujian Province University, Fuzhou 350116, China*

Abstract: Distributed electric propulsion (DEP) uses multiple propellers driven by motors distributed along the leading edge of the wing to produce beneficial aerodynamic interactions. However, the wing will be in the sliding flow of the propeller and the lift and drag characteristics of the wing will change accordingly. The performance of the propeller will also be affected by the wing in its rear. In this paper, combined with wind tunnel tests, the low Reynolds aerodynamic properties of multiple DEP structures are numerically simulated by solving the Reynolds averaged Navier-Stokes (RANS) equation of multiple reference frames (MRF) or slip grid technology. The results demonstrate that the lift and drag of DEP increase in all cases, with the magnitude depending on the angle of attack (AOA) and the relative positions of propellers and wing. When the AOA is less than 16° (stall AOA), the change of lift is not affected by it. By contrast, when the AOA is greater than 16° the *L*/*D* (lift-to-drag ratio) of the DEP system increases significantly. This is because the propeller slipstream delays laminar flow separation and increases the stall AOA. At the same time, the inflow and the downwash effect, which is generated on both sides of the rotating shaft, result in the actual AOA of the wing being greater than the free flow AOA with a fluctuation distribution of the lift coefficient along the span. Also, for the propeller in the DEP, the blocking effect of the wing and the vortex of the trailing edge of the wing result in a significant increase in thrust.

Key words: Distributed electric propulsion (DEP); Aerodynamics; Low Reynolds numbers; Wing interaction

1 Introduction

The concept of distributed electric propulsion (DEP) technology has become one of the most popular in light aircraft research, primarily due to its improved energy conversion efficiency and reduced noise and emissions (Stoll et al., 2014; Gallani et al., 2020). Furthermore, for shorter missions, a higher profit produced by electric aircraft has been noted (Brelje and Martins, 2019; Erhard et al., 2021). Research on the concept of electric propulsion for aircraft in future has already begun (Gohardani et al., 2011; Kong et al., 2018) and has already been adopted by NASA, USA in a training aircraft. It can reduce by approximately 4.8 times the energy required for a traditional aircraft at a selected cruise speed (Borer et al., 2016). The most significant obstacle for electric propulsion aircraft is that the volumetric energy and power density of batteries at present are lower than those for fossil fuel (Liang et al., 2013; Viswanathan and Knapp, 2019). However, DEP can directly fill the wake of the wing to reduce drag, thus reducing energy consumption to achieve the goal of increasing cruising range (Moore and Ning, 2018). There are some other advantages that the DEP method offers, such as high lift at low speed due to the increasing dynamic pressure, and a stable performance due to low gust sensitivity (Kohlman, 1979; Leknys et al., 2018).

Current work on propellers and wing interaction mainly focuses on light aircraft and solar aircraft. Patterson and Borer (2017) used wingtip and high-lift propellers to design a small diameter propeller on the wing leading edge for the X-57 Maxwell aircraft. They studied the aerodynamic characteristics of the high-lift propellers on the aircraft at low flight speed.

✉ Yao LEI, yaolei@fzu.edu.cn
Yao LEI, https://orcid.org/0000-0002-4764-2081
Wen-Jie YANG, https://orcid.org/0000-0001-9356-1090
Yi-yong HUANG, https://orcid.org/0000-0002-4724-6804

Received Apr. 23, 2021; Revision accepted July 25, 2021;
Crosschecked Dec. 23, 2021

Veldhuis and Heyma (2000) proposed an optimization algorithm, based on augmented Lagrange integrals for considering the effect of viscosity, and discussed the aerodynamic optimization of wings in tractor distributed propeller aircraft on the basis of Trefftz-plane analysis. Mian and Wang (2008) and Eslami et al. (2013) studied the flow around the wing of unmanned aerial vehicle (UAV) by using a finite element volume solver and optimizing its airfoil selection. These studies all involved only one-way coupling of the propeller to the wing and therefore it is necessary to conduct a deeper study on the whole structure of DEP.

In this paper, based on the computational fluid dynamics method, the commercial software FLUENT is adopted to numerically simulate the aerodynamic interference in DEP and is compared with wind tunnel tests. Specifically, the aerodynamic variation trend of DEP wings with different structures and their interactions with propellers at low Reynolds number are discussed in detail. Therefore, this paper analyses the aerodynamic performance of DEP, and provides a reference for better design and aerodynamic calculation of propeller aircraft.

2 Theoretical model

The structure of distributed electrically propelled UAVs is shown in Fig. 1. Four propellers are equally distributed on the leading edge of the wing. The dimensionless horizontal distance between the center of rotation of the propeller and the leading edge of the wing is 0.15c (where c is the chord length of the wing). xr ($\Delta x/R$) is the dimensionless vertical distance of the center of the propeller relative to the chord plane of the wing (where R is the radius of propeller and x is the vertical distance between the center of rotation of the propeller and the chord of the wing). A positive value indicates that the propeller is higher than the chord plane.

2.1 Aerodynamics of the propeller

To obtain the aerodynamics of the propeller and the interaction between the adjacent propellers, blade element theory is applied with a high accuracy to consider the geometry, the section direction, and the torsion conditions of the blade (Nguyen et al., 2018). We consider an infinitesimally thin section at the center of the rotor from length y, as shown in Figs. 2 and 3.

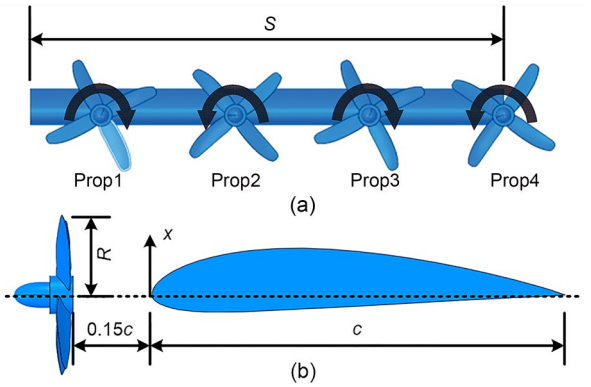

Fig. 1 Construction of DEP aircraft

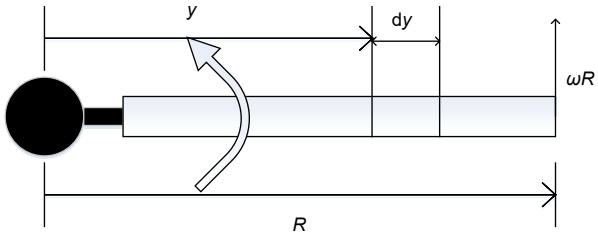

Fig. 2 Model of a blade element. ω is the speed of propeller

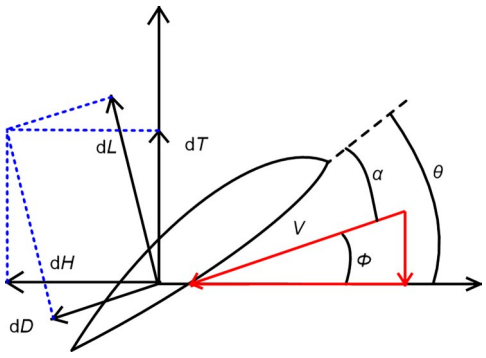

Fig. 3 Vector diagram for a section dr, and length r away from the center of the propeller

Fig. 3 shows the relative inflow velocity V and aerodynamic forces of a blade section. Firstly, dT, dL, dH, and dD represent the differential of thrust, lift, hub force, and drag, respectively. Next, θ is the pitch angle, α the AOA, and Φ the inflow angle. Finally, the thrust coefficient C_T (Kaya and Kutay, 2014; Nguyen et al., 2018) and thrust T are defined as

$$C_T = \frac{1}{2\pi}\int_0^R\int_0^{2\pi}\frac{\Delta F_T}{\rho A(\omega R)^2}\,\mathrm{d}\Psi\mathrm{d}y, \tag{1}$$

$$T = C_T \rho A(\omega R)^2, \tag{2}$$

where Ψ is the azimuth of the propeller blade, A is the rotor disk area, ω is the rotate speed, ΔF_{T} is the total vertical forces acting on the blade, and ρ is the density of air.

The rotor inflow ratio μ and the advance ratio λ under generalized motion are defined as

$$\mu = \frac{V_\infty \cos\alpha}{\omega R}, \tag{3}$$

$$\lambda = \frac{V_\infty \sin\alpha + v}{\omega R}, \tag{4}$$

where V_∞ is the freestream velocity and v is the total velocity.

Assuming that the installation angle of the blade profile changes linearly,

$$\theta = \theta_0 + \theta_{\mathrm{tw}} r, \tag{5}$$

where θ_0 is the zero pitch angle and θ_{tw} is the twist angle.

Then the isolated rotor thrust coefficient under generalized motion is given as

$$\frac{C_T}{\sigma\alpha} = \left(\frac{1}{6} + \frac{1}{4}\mu^2\right)\theta_0 + (1+\mu^2)\frac{\theta_{\mathrm{tw}}}{8} - \frac{1}{4}\lambda, \tag{6}$$

$$T = \sigma\alpha\left[\left(\frac{1}{6} + \frac{1}{4}\mu^2\right)\theta_0 + (1+\mu^2)\frac{\theta_{\mathrm{tw}}}{8} - \frac{1}{4}\lambda\right]\rho A(\omega R)^2, \tag{7}$$

where σ is the rotor's solidity.

2.2 Aerodynamics of the wing

For a wing with a large sweep angle or a small span, the lift line theory and profile assumptions are no longer able to correctly represent the actual flow and to calculate its aerodynamic characteristics. In such cases, they must be calculated using lift surface theory. However, it is difficult to find the lift surface equation by analytical methods. The vortex lattice method is assumed as a practical numerical calculation method in the lift surface theory. Firstly, when the point vortex of circulation strength Γ, air density, and inflow velocity are determined, L is acquired by the Kutta-Joukowski theorem:

$$L = -\rho V_\infty \Gamma. \tag{8}$$

According to the definition of the lift coefficient, there is:

$$\mathrm{d}\Gamma(z_j) = -\frac{1}{2} V_\infty c_{\mathrm{l}j} c_j. \tag{9}$$

In the equation, c_j is the chord length of the section j, $c_{\mathrm{l}j}$ is the lift coefficient of the wing section j (i.e. the section at z_j), and $\mathrm{d}\Gamma(z_j)$ is the circulation strength component of all the lattice wings (i=1, 2, $\cdots$, I) on the section j, i is the section along the chord, j is the section along the wingspan and I and J are the total numbers of sections i and j, respectively. Then, according to $\gamma_{ij} = -\Gamma_{ij}/lV_\infty$,

$$\mathrm{d}\Gamma\left(z_j\right) = -lV_\infty \sum_{i=1}^{I} \gamma_{ij}, \tag{10}$$

where γ_{ij} is the horseshoe vortex on the lattice wing (i, j), l is the length of γ_{ij}, and Γ is the circulation strength on the lattice wing (i, j).

Then the profile lift coefficient is:

$$c_{\mathrm{l}j} = \frac{2l}{c_j} \sum_{i=1}^{I} \gamma_{ij}. \tag{11}$$

The lift of the unit length of each profile is $\mathrm{d}L/\mathrm{d}z = \rho V_\infty^2 c_{\mathrm{l}j} c_j/2$; therefore, the total lift and lift coefficient of the wing are:

$$L = \frac{1}{2}\rho V_\infty^2 \sum_{j=1}^{J} c_{\mathrm{l}j} c_j \Delta z_j, \tag{12}$$

$$C_{\mathrm{l}} = \frac{L}{\frac{1}{2}\rho V_\infty^2 S} = \frac{1}{S}\sum_{j=1}^{J} c_{\mathrm{l}j} c_j \Delta z_j, \tag{13}$$

where Δz_j is the length of the section j and S is the area of the wing.

2.3 Interference between propeller and wing

The aerodynamic interference of the DEP system is very complicated to obtain. Based on the lift line theory or the lift surface theory, the wing lift distribution is calculated using the Fourier coefficient of the semi-infinite series. Patterson and German (2015) assumed that there is an incompressible flow, and built a wing lift incremental model based on the thin wing theory. The aerodynamic interference is shown in Fig. 4.

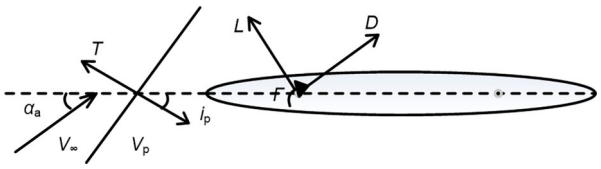

Fig. 4 Two-dimensional point vortex model

The slipstream is considered to cover the entire wing, and V_p is the propeller slipstream velocity. The wing is seen to be subjected to a single point vortex with circulation strength Γ at a 1/4 chord length and produces a downward induced velocity at 3/4 chord length.

Fig. 5 shows a change of effective AOA α_{ep}, which is caused by the propeller slipstream.

The effective velocity $\boldsymbol{V}_{ep}$ acting on the wing is the vector sum of $\boldsymbol{V}_\infty$ and $\boldsymbol{V}_p$. Without the interaction of the propeller, $\boldsymbol{W}_\infty$ is the downward induced velocity from the point vortex. When affected by the propeller slipstream, the downward induced velocity will change to $\boldsymbol{W}_{new}$. When the direction of the propeller slipstream is inclined downward, as shown in Fig. 5a, the circulation will decrease relative to that without the propeller because $\boldsymbol{W}_{new}<\boldsymbol{W}_\infty$ and the AOA of airfoil is decreased. The lift vector is tilted in the direction of drag at angle $\alpha_a-\alpha_{ep}$ (where α_a is the AOA of wing), so the force produced by the wing is not all beneficial for lift and some directly increases drag. When the slipstream of the propeller is aligned with the airfoil chord line (i_p=0) as shown in Fig. 5b, $\boldsymbol{W}_{new}$ will be equal to $\boldsymbol{W}_\infty$. When $\boldsymbol{V}_p$ is aligned with $\boldsymbol{V}_\infty$ as shown in Fig. 5c, $\boldsymbol{W}_{new}$ is larger than $\boldsymbol{W}_\infty$, so the circulation will increase and this will improve the lift of the wing. As Fig. 5d shows, both the circulation strength and AOA of airfoil will increase along with the increased $\boldsymbol{V}_p$ where $-i_p>\alpha_a$. However, this will lead to decreased lift if the propeller is tilted forward.

According to Eq. (8), the lift per unit span caused by only freestream velocity is $L'=\rho V_\infty \Gamma_\infty$, and the lift per unit span caused by propeller slipstream is $L'_\infty=\rho V_\infty \Gamma_\infty$. Γ_∞ is the circulation strength along with $\boldsymbol{V}_\infty$. The change of lift is $L'_{new}=\rho V_{ep}\Gamma_{new}$. The percentage increase of lift can be expressed as: $\Delta L'=L'_{new}-L'_\infty$, if the circulation strength increases or decreases by the factor of circulation strength increase, κ. The circulation strength $\Gamma=\pi c W$ (where W is the induced velocity), so

$$\kappa=\frac{W_{new}}{W_\infty}=1-\frac{V_p \sin i_p}{V_\infty \sin\alpha_a}. \tag{14}$$

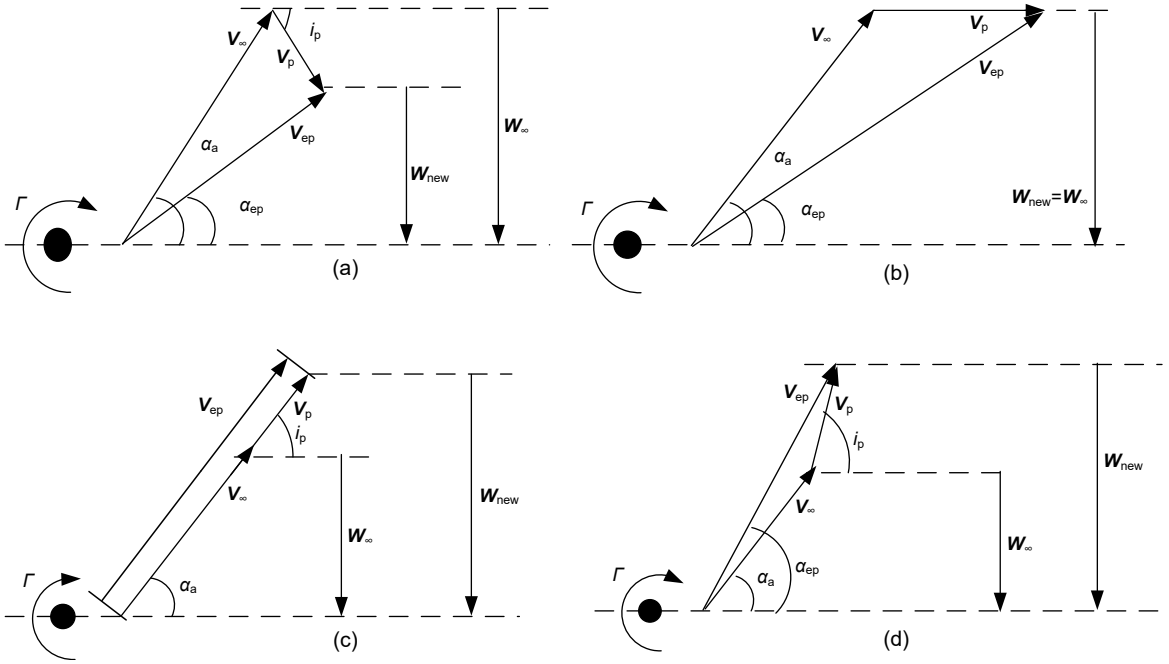

Fig. 5 Vector diagrams of the effective AOA under various directions of the propeller slipstream: (a) V_p inclined downward, $i_p>0$; (b) V_p aligned with the airfoil chord line, $i_p=0$; (c) V_p aligned with V_∞, $i_p=-\alpha_a$; (d) V_p inclined upward and $-i_p>\alpha_a$

Patterson and German (2015) modeled the effects of various direction of slipstream to airflow lift, but the lift has a tendency to decrease with the height of the slipstream. Patterson and German (2015) suggested that the effect of a limited slipstream height on lift reduction could effectively be simulated as a simple reduction in slipstream velocity (Patterson et al., 2016). Therefore, a correction factor, β ($0\leqslant\beta\leqslant1$), is defined to correct the velocity V_p caused by the propeller, i.e. βV_p. For the cases shown in Fig 5, the percentage increases of lift are given by Eq. (15):

$$\frac{\Delta L'}{L'_\infty}=\left(1-\frac{\beta V_p\sin i_p}{V_\infty\sin\alpha_a}\right)\times\frac{\sqrt{V_\infty^2+2V_\infty\beta V_p\cos\left(\alpha_a+i_p\right)+\left(\beta V_p\right)^2}}{V_\infty}-1,\quad i_p>0, \tag{15a}$$

$$\frac{\Delta L'}{L'_\infty}=\frac{\sqrt{V_\infty^2+2V_\infty\beta V_p\cos\left(\alpha_a\right)+\left(\beta V_p\right)^2}}{V_\infty}-1,\quad i_p=0, \tag{15b}$$

$$\frac{\Delta L'}{L'_\infty}=\frac{\beta V_p}{V_\infty}\left(\frac{\beta V_p}{V_\infty}+2\right),\quad i_p=-\alpha_a, \tag{15c}$$

$$\frac{\Delta L'}{L'_\infty}=\kappa\frac{\beta V_p}{V_\infty}-1,\quad -i_p>\alpha_a, \tag{15d}$$

where $\kappa>1$.

3 Computational-fluid-dynamics analysis

3.1 Simulation setup

The DEP in this paper consists of a wing with a length of 0.3 m and a chord length of 0.15 m, four propellers with a diameter and pitch of 91.44 cm. The wing is a standard NACA4415 airfoil. The influence of the propeller position on the wing is mainly divided into two factors: the streamwise position and the vertical position. Various different DEP structures are numerically simulated with ANSYS. The Navier-Stokes equation model is applied to analyze the characteristics of the external flow field. Moreover, the mesh refinement is performed on regions with a large gradient of physical field flow. Additionally, the finite volume method is used to discretize the differential equations. Considering the low Reynolds number environment, the Spalart-Allmaras model is selected to obtain the flow field of DEP (Aref et al., 2018). The pressure correction is performed using the semi-implicit method for pressure linked equations (SIMPLE) algorithm, and the pressure interpolation is selected in the standard format. Momentum, energy equation, and turbulent viscosity are all in the second-order upwind discrete format. The boundary conditions were set to a propeller speed of 18 000 r/min, a speed inlet of 18 m/s, and a standard pressure outlet. Lastly, the sliding grid is applied to deal with the interaction between the rotating and the stationary regions, and then the steady state calculation result of the multiple reference frame (MRF) method is applied as the initial condition for the slip mesh transient calculation. The mesh distribution is shown in Fig. 6.

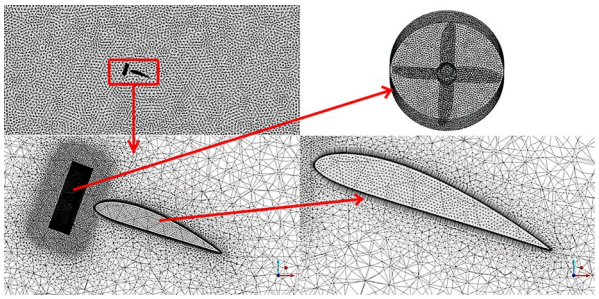

Fig. 6 Mesh distribution

Four different grid densities were used to verify the grid independence as shown in Table 1.

Table 1 Comparison of various grid computational and test results of xr0-0.15*c* configuration at AOA of 20°

Rotate region grid ($\times10^5$)	Total grid ($\times10^5$)	C_l	C_l error (%)	C_d	C_d error (%)
1.89	85.47	1.142	−14.2	0.318 35	+5.8
2.14	107.51	1.186	−10.9	0.310 22	+3.1
2.55	133.64	1.218	−8.5	0.308 84	+2.6
2.83	167.29	1.219	−8.4	0.308 42	+2.5

It is clear that the error of drag coefficient is less than 5.8% in all grids, but the lift coefficient error is more than 10% in the sparse grid. The third grid presents better accuracy on lift coefficient C_l and drag coefficient C_d at fewer grid quantities. Furthermore, we did the validation for the used CFD methodology we use by comparison of C_l and C_d obtained both in experiment and simulation (Lei and Ye, 2020). Results showed that they were generally in good agreement.

3.2 Simulation results

The tractor structure of DEP system indicated that the propellers are installed in front of the wing. Fig. 7 shows the vector distribution of the 43% span section of the tractor structure at xr0-0.15*c* and isolated wing at AOA of 8° and 20°.

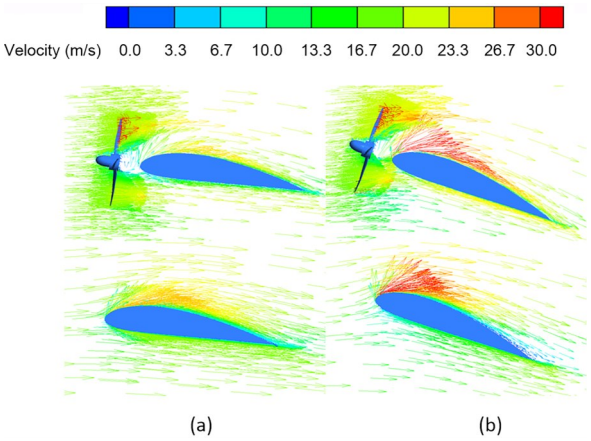

Fig. 7 Velocity vector distribution: (a) AOA is 8°; (b) AOA is 20°

It can be seen that the downwash of the propeller changes the original direction of motion when encountering the leading edge of the wing, finally forming a vortex in the middle and flowing around the wing. This significantly increases the interaction of the airflow with the upper and lower surfaces of the wing compared to the individual wings. In addition, the laminar separation bubble at the trailing edge of the wing disappears due to the slipstream from the propeller, optimizing the aerodynamic performance of the wing. As the airflow passes through the plane formed by the blades, the momentum of the planar tubular airflow of the propeller is increased, resulting in a propeller slipstream that causes the flow state of the wing to change. Since the slipstream injects energy into the airflow, the static pressure and dynamic pressure of the wing will increase, eventually leading to an increase in lift, induced drag, and local circulation. The local AOA of the wing also changes under the action of the swirling airflow. The generation of propeller slipstream phenomenon mainly includes the contraction of the slipstream tubular airflow and the viscosity of the airflow. The wing behind the propeller also affects the flow of the propeller slipstream, causing airflow obstruction and side wash.

Fig. 8 shows a pressure contour of various DEP structures at 8° and 20° AOA compared with the isolated wing.

At AOA of 8°, the pressure distribution of xr0-0.15*c* is different from that of an interference-free wing, since the pressure of the upper surface of the airfoil is reduced and the pressure of the lower surfaces is increased caused by the interaction of propeller slipstream with the leading edge of the wing. However, the DEP system does not present better lift performance at a smaller AOA. At AOA of 20°, the low-pressure area formed significantly and the high-pressure area is also enhanced in places, which directly increases wing lift and drag. Comparing (d) and (e) in Fig. 8, it can be seen that there is no significant difference in the pressure distribution on the wing when the distance of propeller center to leading edge is 0.15*c* to 0.2*c*. Furthermore, the installation distance will affect the performance of the propeller. Comparing (d), (f), (g), and (h) in Fig. 8, the vertical installation position of the propeller significantly changes the DEP flow field distribution. When the central axis of the propeller is above the chord, the low-pressure region of the wing decreases and connects with the low-pressure area of the propeller. Simultaneously, the area effected by the propeller slipstream on the lower surface of the airfoil is reduced and the high-pressure region is weakened, thus finally reducing the lift performance. When the central axis of the propeller is located below the chord, the high-pressure area moves slightly towards the trailing edge, and the upper surface is closer to the high-speed slipstream area to increase flow velocity and then improve lift performance. In short, the aerodynamic performance of the tractor is affected by the vertical installation position of the propeller, and the vertical offset from the bottom up makes the wing lift gradually decrease.

Considering that the configuration of xr0-0.15*c* did well on pressure difference between upper and lower surfaces of airfoil, various AOAs were simulated to obtain the trend line of lift coefficient and drag coefficient with AOA as shown in Fig. 9.

It can be seen from Fig. 9a that when the AOA is less than 20°, the lift coefficient increases linearly with the increase of the AOA. When it is greater than 20°, it tends to be stable. Moreover, the drag increases with the increase of the AOA, reaching a maximum of 0.585

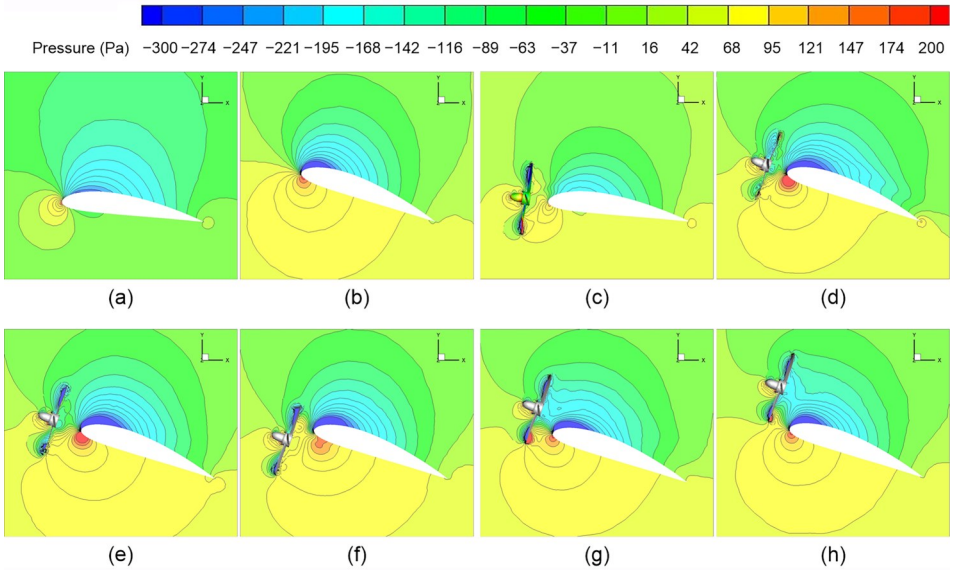

Fig. 8 Pressure distributions: (a) isolated wing at AOA of 8°; (b) isolated wing at AOA of 20°; (c) xr0-0.15*c* at AOA of 8°; (d) xr0-0.15*c* at AOA of 20°; (e) xr0-0.2*c* at AOA of 20°; (f) xr−0.5-0.15*c* at AOA of 20°; (g) xr0.5-0.15*c* at AOA of 20°; (h) xr1-0.15*c* at AOA of 20°

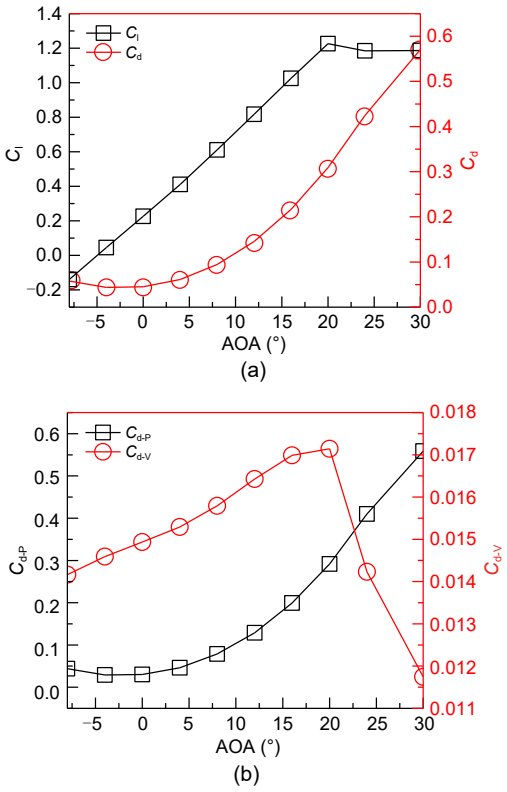

Fig. 9 C_l and C_d variations of tractor at xr0-0.15*c*

at 30°. With the influence of the propeller slipstream, the lift and drag of the wing increase significantly at high AOA, and as the AOA increases, the trend of lift increases is gradually weakened, and the trend of increasing drag is always strong. The wing drag is derived from two parts, the differential of pressure drag ($C_{d\text{-}P}$) and the viscous drag ($C_{d\text{-}V}$). Fig. 9b shows the two drag changes with the AOA. The difference of pressure drag is much larger than the viscous drag. The trend of $C_{d\text{-}P}$ with the AOA is exactly the same as the total drag in Fig. 9a, indicating that the drag of the wing is mainly derived from the differential pressure drag. The viscous drag drops sharply after 20°, which reduces the total drag of the tractor at a high AOA to a certain extent, further reflecting the advantages of the DEP system.

At an AOA of 8°, the lift coefficient distribution of xr0-0.15*c*/0.2*c* and isolated wing along spanwise is shown in Fig. 10.

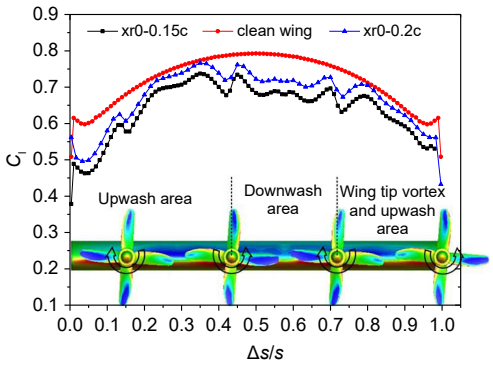

Fig. 10 C_l distribution along the span at AOA of 8°. $\Delta s/s$ is the wing section along the spanwise of the wing

It is clear that the DEP system did not give better lift performance than the isolated wing at an AOA of 8°. For the upwash and downwash caused by the rotation of propeller, the slipstream produced greater influence on the lift of the wing. The general lift coefficient of DEP system is a significant increase in the 0.05 s to 0.35 s upwash area, next a slow decrease in the downwash area, and finally a gradual reduction in the area where the wing tip vortex interacts with the slipstream. The lift coefficient shows a significant decrease at the center of rotation of the left three propellers, which may be caused by lower slipstream velocity in the area, and indirectly decreases the circulation strength of this airfoil section. It is obvious that the configurations of xr0-0.15*c* and xr0-0.2*c* show the same trend of lift coefficient distribution spanwise. This demonstrates that at the same vertical mounting position of the propeller, the trend of lift coefficient distribution does not change with horizontal distance. However, the slipstream velocity will be affected by the shorter horizontal distance and will decrease lift performance eventually.

Fig. 11 shows the lift coefficient distributions of various configurations along the span at 20° AOA.

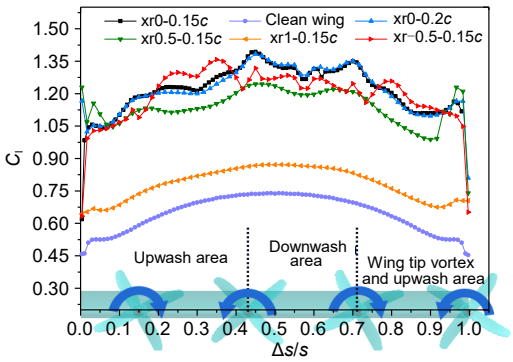

Fig. 11 C_l distributions along the span at AOA of 20°

It is clear that the lift of this airfoil does not perform well at the 20° AOA, but four DEP configurations significantly increase the lift performance except for xr1-0.15*c*. This is due to the propeller slipstream decreasing the effective AOA and increasing the effective velocity. The lift coefficient trend is similar to that of an isolated wing when the propeller vertical upward offset is *R*, because the area under the effect of propeller slipstream is limited, but the velocity of upper surface of the airfoil increased by the propeller improves lift. The xr0.5−0.15*c* configuration also presents lower lift performance than when the propeller is aligned with, or under, the chord line. It is indicated that when the propeller is installed under, or is aligned with, the chord line, the DEP system has a better lift performance at a higher AOA. Obviously, the xr0-0.15*c* and xr0-0.2*c* have similar lift performances and both of them are better than xr–0.5-0.15*c* at a 20° AOA.

As we analyzed earlier, the propeller slipstream can increase wing lift. In addition, the reaction of the wing to the propeller also affects the propeller thrust performance. Fig. 12 shows the thrust of the four propellers in the xr0-0.15*c* configuration as a function of the AOA of the wing.

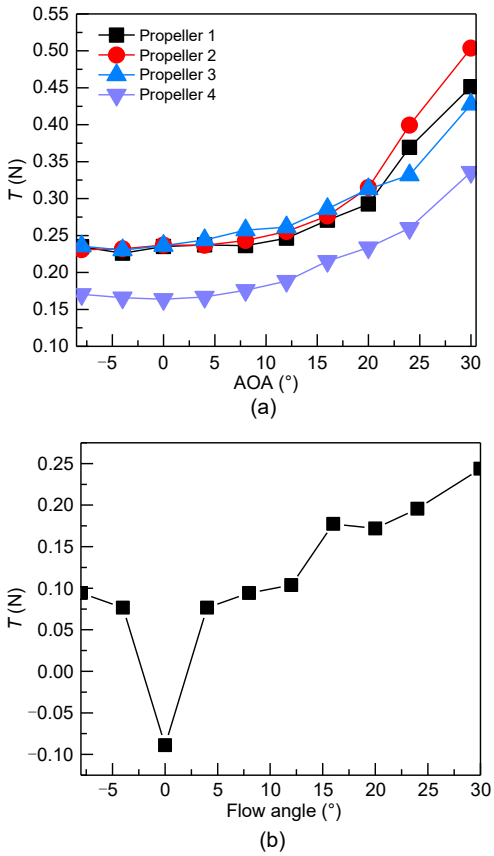

Fig. 12 Thrust distributions: (a) xr0-0.15*c*; (b) single propeller

The thrust is increased with the AOA. The propellers are distributed at the same spacing along spanwise, and the order of the propeller along spanwise is 1, 2, 3, and 4. The position of No. 4 is at the wing tip. The No. 4 propeller has a smaller thrust than others because only half of the paddle is in front of the wing. However, comparing the thrust distribution of a single

propeller as shown in Fig. 12b, it can be seen that the propeller thrust in the DEP is always greater than that of the propeller that is not affected by the wing, and the maximum thrust performance is doubled in this case. For the propeller slipstream, the wing located downstream of the propeller will exert a reaction force on the propeller by the pressure field, which will affect the propeller thrust. This effect is called the blocking effect. It causes the airflow speed through the propeller paddle to be less than the far forward flow velocity, and the actual working state of the propeller changes. According to Eq. (4), the advancement ratio (λ) of the propeller is lowered, but the advancement ratio (λ_i) of the thrust portion is increased, and thereby increases the thrust of the propeller. The rectification of the wing to the propeller slipstream is also an important reason affecting the aerodynamic characteristics of the propeller. A large part of the energy consumed by the propeller is used to form a swirling vortex of air, and the tangential velocity of the vortex does not contribute to the propeller pull. The rectification of the wing reduces the energy loss caused by the vortex, thereby increasing the propeller's thrust and effectiveness. However, this will inevitably lead to changes in the aerodynamic characteristics of the wing. In fact, due to the rotation of the propeller, the speed of the blade on the upward movement side is reduced, and the speed of the downward movement of the blade is increased, resulting in different thrust of the blade at different phases, with periodic fluctuations.

4 Experiments

4.1 Experimental setup

In order to verify the validity of the simulation, a test bench was constructed as shown in Fig. 13. Motors and propellers are decoupled from the wing in order to study the aerodynamic effects. Independent revolution per minute (RPM) sensors are used to measure the thrust four propellers, and each motor is controlled by a motor controller. ATI Gamma F&T sensor is attached to the isolated wing to measure force. The design is adjustable to study various motor positions and propellers in pusher and tractor configurations separately. The wind tunnel cross-section is 0.6 m×0.6 m, and wing span is half the height of the wind tunnel allowing the capture of 3D effects such as tip vortices.

The DEP configuration is shown in Fig. 14. NACA4415 airfoil is adopted as the wing with the length of span is 0.3 m, the chord is 0.15 m, and the aspect ratio is 2. Four propellers were mounted along the wing span, the diameter of propeller is 0.9144 m, the pitch is 0.9144 m, and the number of blades is 4. The propeller rotation directions are as shown in Fig. 1. In this test, the free-stream speed is 18 m/s (typical), the rotate speed of propeller is 18 000 r/min, and the Reynolds number of wing is around 180 000.

4.2 Experimental results

Fig. 15 shows the comparison of experimental and simulation results with various horizontal position

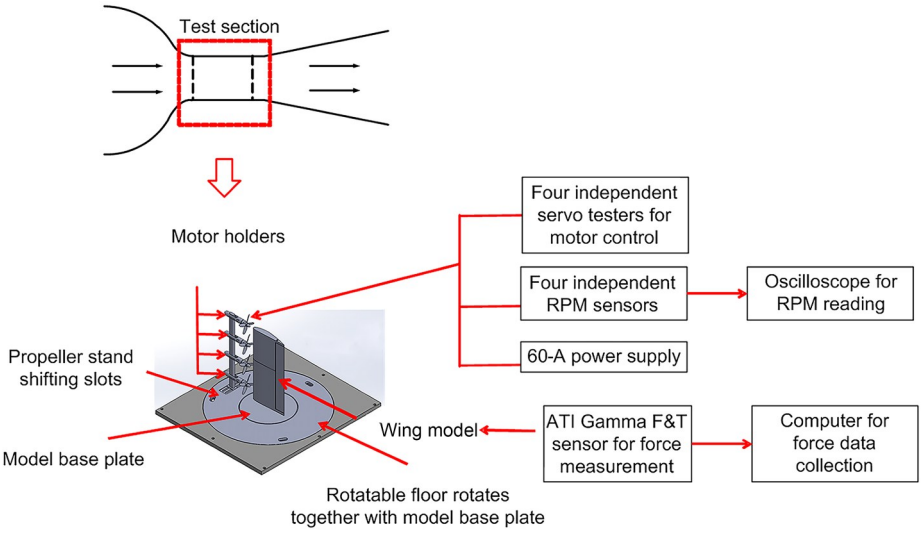

Fig. 13 Experimental setup

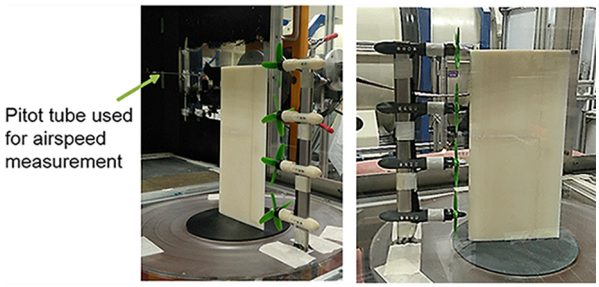

Fig. 14 DEP experimental design

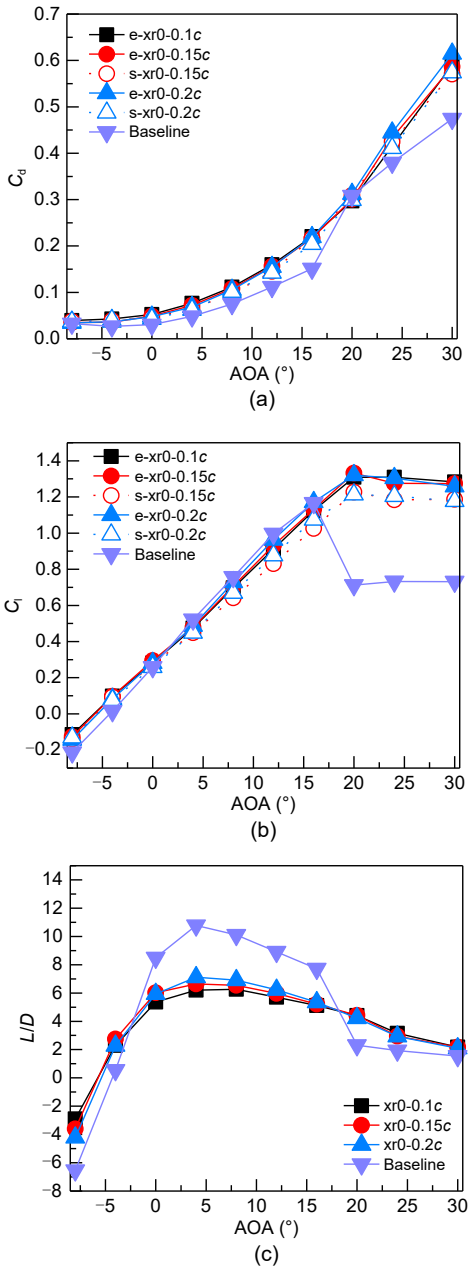

Fig. 15 Experimental and simulation results of tractor: (a) C_d; (b) C_l; (c) L/D

and vertical offset x/R=0, where s is short for simulation and e is short for experiment.

Comparing with the experimental results, the error range of CFD in the calculation of lift and drag is within 10%. As shown in Figs. 15a and 15b, the aerodynamic characteristics of the tractor-type wing and the wing without propeller interaction at different AOAs are obtained. It can be seen that the common feature of both is that, as the AOA increases, the lift coefficient and drag coefficient also increase. In terms of lift coefficient, when the AOA is less than 16°, the lift coefficient curves approximately coincide on one curve, and the lift characteristics have not been improved. When the AOA is greater than 20°, the tractor lift curve begins to stabilize, while the wing without the propeller has stalled at this time, and the lift coefficient drops significantly from 1.1718 to 0.7300. As far as the drag coefficient in Fig. 15b is concerned, the drag coefficient of the tractor has different degrees of increase at different AOAs compared to the drag coefficient of the wing without the propeller. According to the previous section, this may be due to the blocking effect between the propeller and the wing, and the effect of the slipstream on the upper and lower surfaces of the wing. The design of the tractor structure has a relatively obvious role in preventing the airflow of the boundary layer from slipping at the high AOA and thus preventing the stall of the wing. However, for a wing with a lower AOA, the tractor structure does not have a significant effect on improving aerodynamic performance. From the longitudinal direction of the curve, the influence of the flow direction of different propellers on the lifting drag of the wing is small. Also, as can be seen from Fig. 15c, a tractor DEP system results in increased L/D at lower AOA when further away from the leading edge. Delay of stall and an absence of a loss of lift at high AOA is the biggest benefit, but this comes at the cost of an almost halved L/D at lower AOAs. Comparing the results of the numerical simulation in Fig. 9a, it can be found that the difference between the test result and the simulation result is within 5%, which proves the effectiveness of the simulation.

With the horizontal position fixed at 0.15c, comparisons of the experimental and simulation of various vertical offset x/R configuration results are shown in Fig. 16.

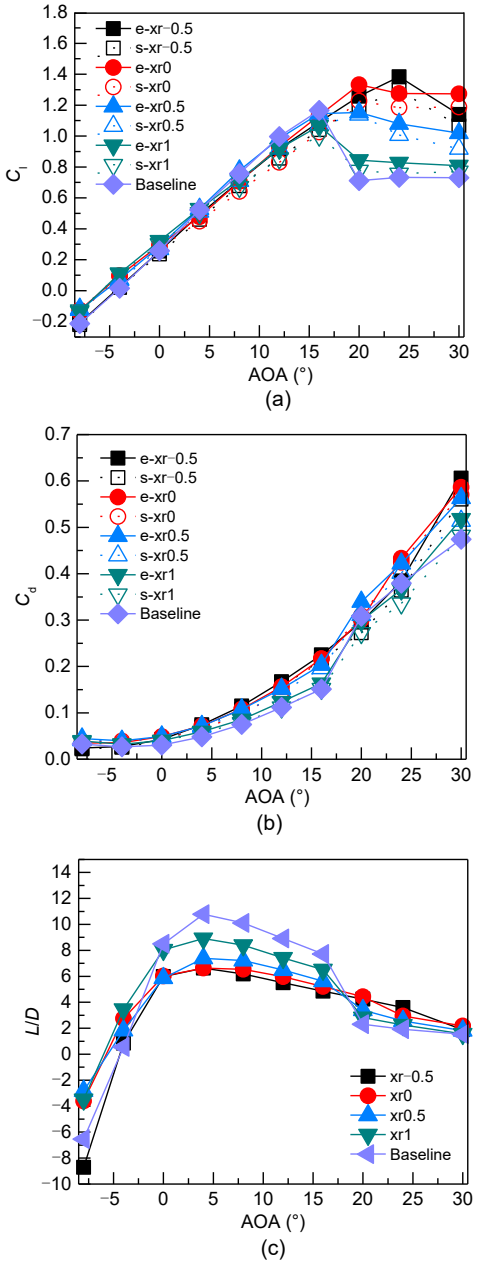

Fig. 16 Experimental result of tractor: (a) C_l; (b) C_d; (c) L/D

Similarly, when the AOA is less than 16°, the effect of the propeller slipstream on the wing is not obvious. At this time, the upwash effect and the downwash action of the blade rotation on the wing have a tendency to cancel each other. The speed increases the effect of the slip zone of the propeller and increases the speed of the upper and lower surfaces. Although the negative pressure on the upper surface is increased, the positive pressure on the lower surface is reduced. Finally, more pressure difference gained with higher lift increased. When the AOA is greater than 16°, the wing without the slipstream has stalled, and the overall trend of the DEP wing is an increase in lift. However, according to the numerical simulation results in the previous section, the change of the vertical installation position of the propeller will have different effects on the rear wing. The experimental results also show that the lift of DEP varies at high AOAs due to changes in vertical offset. It can be roughly described that the propeller mounting position is from top to bottom, and the lift performance is gradually increased. In the xr1 structure, the increase in lift is also minimal, and the lift coefficient does not increase by more than 0.1. Similarly, corresponding to the drag coefficient curves in Fig. 16b, the xr1 drag is not significantly increased except for 30°. The other structural drag coefficients are larger than the baseline, but the overall increase in drag is small due to the vertical offset change. From the point of view of the L/D curve in Fig. 16c, L/D is improved at lower AOA due to the decreasing drag when the propeller is located above the wing chord line.

5 Conclusions

This paper first gives an aerodynamic model of propeller, wing, and their mutual interference. Then, the aerodynamic performance of the DEP system is studied by wind tunnel tests and numerical simulations. Finally, the aerodynamic interference between propeller and wing with different structures is studied in detail. The conclusions of this paper are as follows:

1. When the AOA is less than 16° (stall AOA), the lift of the DEP system is not sensitive to the AOA. For a smaller AOA, it still maintains a linear relationship. When the AOA is greater than 16°, the lift without the propeller is greatly reduced due to the stall, and the lift of the DEP system is significantly improved, which can be increased by about 73%–87%. The DEP drag is always higher than that on the isolated wing.

2. The acceleration of the axial airflow by the propeller, and the effect of the upwash and downwash induced by the slipstream may cause the aerodynamic force of the wing to exhibit an increase in lift and

drag. The wing of the tractor structure has a decrease in L/D when the AOA is less than 16°, whereas the L/D is significantly increased at the same time.

3. The tractor DEP system presents higher lift and L/D at negative and high AOAs, which means the distance of climb and descending will decrease and require less energy. Delay of stall and an absence of a loss of lift at high AOA is the biggest benefit, but it may lead to a lower L/D of the DEP system compared with the isolated wing at lower AOAs. This is also a disadvantage for cruising, and we can retract part of the propellers during cruising to reduce cruising drag.

Acknowledgments

This work is supported by the National Natural Science Foundation of China (No. 51505087) and the Fujian Provincial Industrial Robot Basic Components Technology Research and Development Center (No. 2014H2004), China.

Author contributions

Yao LEI designed the research and processed the corresponding data. Wen-jie YANG wrote the first draft of the manuscript and performed the CFD simulations. Yi-yong HUANG helped to organize the wind tunnel tests.

Conflict of interest

Yao LEI, Wen-jie YANG, and Yi-yong HUANG declare that they have no conflict of interest.

References

Aref P, Ghoreyshi M, Jirasek A, et al., 2018. Computational study of propeller–wing aerodynamic interaction. *Aerospace*, 5(3):79. https://doi.org/10.3390/aerospace5030079

Borer NK, Patterson MD, Viken JK, et al., 2016. Design and performance of the NASA SCEPTOR distributed electric propulsion flight demonstrator. 16th AIAA Aviation Technology, Integration, and Operations Conference. https://doi.org/10.2514/6.2016-3920

Brelje BJ, Martins JRRA , 2019. Electric, hybrid, and turboelectric fixed-wing aircraft: a review of concepts, models, and design approaches. *Progress in Aerospace Sciences*, 104:1-19. https://doi.org/10.1016/j.paerosci.2018.06.004

Erhard RM, Clarke MA, Alonso JJ, 2021. A low-cost aeropropulsive analysis of distributed electric propulsion aircraft. AIAA Scitech 2021 Forum. https://doi.org/10.2514/6.2021-1200

Eslami E, Tadjfar M, Najafi S, 2013. Aerodynamic performance of Parastoo UAV. *Aircraft Engineering and Aerospace Technology*, 85(2):97-103. https://doi.org/10.1108/00022661311302706

Gallani MA, Goes LCS, Nerosky LAR, 2020. Effects of distributed electric propulsion on the performance of a general aviation aircraft. AIAA Propulsion and Energy 2020 Forum. https://doi.org/10.2514/6.2020-3594

Gohardani AS, Doulgeris G, Singh R, 2011. Challenges of future aircraft propulsion: a review of distributed propulsion technology and its potential application for the all electric commercial aircraft. *Progress in Aerospace Sciences*, 47(5):369-391. https://doi.org/10.1016/j.paerosci.2010.09.001

Kaya D, Kutay AT, 2014. Aerodynamic modeling and parameter estimation of a quadrotor helicopter. AIAA Atmospheric Flight Mechanics Conference. https://doi.org/10.2514/6.2014-2558

Kohlman DL, 1979. Flight test results for an advanced technology light airplane. *Journal of Aircraft*, 16(4):250-255. https://doi.org/10.2514/3.58513

Kong XH, Zhang ZR, Lu JW, et al., 2018. Review of electric power system of distributed electric propulsion aircraft. *Acta Aeronautica et Astronautica Sinica*, 39(1):46-62 (in Chinese). https://doi:10.7527/s1000-6893.2017.21651

Lei Y, Ye YQ, 2020. Aerodynamic characteristics of a hexrotor MAV with three coaxial rotors in hover. *IEEE Access*, 8:221312-221319. https://doi.org/10.1109/ACCESS.2020.3042797

Leknys RR, Arjomandi M, Kelso RM, et al., 2018. Leading-edge vortex development on a pitching flat plate with multiple leading edge geometries. *Experimental Thermal and Fluid Science*, 96:406-418. https://doi.org/10.1016/j.expthermflusci.2018.03.001

Liang JY, Zhang JL, Zhang X, et al., 2013. Energy management strategy for a parallel hybrid electric vehicle equipped with a battery/ultra-capacitor hybrid energy storage system. *Journal of Zhejiang University-SCIENCE A (Applied Physics & Engineering)*, 14(8):535-553. https://doi.org/10.1631/jzus.A1300068

Mian AA, Wang DB, 2008. Dynamic modeling and nonlinear control strategy for an underactuated quad rotor rotorcraft. *Journal of Zhejiang University-SCIENCE A*, 9(4): 539-545. https://doi.org/10.1631/jzus.A071434

Moore KR, Ning A, 2018. Distributed electric propulsion effects on existing aircraft through multidisciplinary optimization. AIAA/ASCE/AHS/ASC Structures, Structural Dynamics, and Materials Conference. https://doi.org/10.2514/6.2018-1652

Nguyen DH, Liu Y, Mori K, 2018. Experimental study for aerodynamic performance of quadrotor helicopter. *Transactions of the Japan Society for Aeronautical and Space Sciences*, 61(1):29-39. https://doi.org/10.2322/tjsass.61.29

Patterson MD, German BJ, 2015. Simplified aerodynamics models to predict the effects of upstream propellers on wing lift. 53rd AIAA Aerospace Sciences Meeting. https://doi.org/10.2514/6.2015-1673

Patterson MD, Borer NK, 2017. Approach considerations in

aircraft with high-lift propeller systems. 17th AIAA Aviation Technology, Integration, and Operations Conference.
https://doi.org/10.2514/6.2017-3782

Patterson MD, Derlaga JM, Borer NK, 2016. High-lift propeller system configuration selection for NASA's SCEPTOR distributed electric propulsion flight demonstrator. 16th AIAA Aviation Technology, Integration, and Operations Conference.
https://doi.org/10.2514/6.2016-3922

Stoll AM, Bevirt J, Moore MD, et al., 2014. Drag reduction through distributed electric propulsion. 14th AIAA Aviation Technology, Integration, and Operations Conference.
https://doi.org/10.2514/6.2014-2851

Veldhuis LLM, Heyma PM, 2000. Aerodynamic optimisation of wings in multi-engined tractor propeller arrangements. *Aircraft Design*, 3(3):129-149.
https://doi.org/10.1016/S1369-8869(00)00010-0

Viswanathan V, Knapp BM, 2019. Potential for electric aircraft. *Nature Sustainability*, 2(2):88-89.
https://doi.org/10.1038/s41893-019-0233-2